

**Chaos and Complex Systems - CCS2010**  
3<sup>rd</sup> International Interdisciplinary Chaos Symposium  
Istanbul, Turkey, 21-24 May 2010.

# Self-Organized Criticality in Solar Physics and Astrophysics

Markus J. Aschwanden

*Solar and Astrophysics Laboratory, Lockheed Martin, Palo Alto, USA - e-mail:  
aschwanden@lmsal.com*

## Abstract

The concept of “self-organized criticality” (SOC) has been introduced by Bak, Tang, and Wiesenfeld (1987) to describe the statistics of avalanches on the surface of a sandpile with a critical slope, which produces a scale-free powerlaw size distribution of avalanches. In the meantime, SOC behavior has been identified in many nonlinear dissipative systems that are driven to a critical state. On a most general level, SOC is the statistics of coherent nonlinear processes, in contrast to the Poisson statistics of incoherent random processes. The SOC concept has been applied to laboratory experiments (of rice or sand piles), to human activities (population growth, language, economy, traffic jams, wars), to biophysics, geophysics (earthquakes, landslides, forest fires), magnetospheric physics, solar physics (flares), stellar physics (flares, cataclysmic variables, accretion disks, black holes, pulsar glitches, gamma ray bursts), and to galactic physics and cosmology.

Keywords: astrophysics - nonlinear dynamics - statistics - selforganized criticality  
- solar flares

## 1 Introduction

Physical processes in our universe can be subdivided into incoherent and coherent processes. Examples of incoherent processes are fractional Brownian motion, diffusion, collisional plasma processes, plasma heating, which all are governed by random processes and thus can be described by binomial and Poissonian statistics, which exhibit exponential-like or Gaussian-like distributions. In contrast, coherent processes overcome the threshold of the random noise background and grow in a multiplicative way, such as avalanches, chain reactions, or catastrophes, which all exhibit powerlaw-like size distributions. The dichotomy of incoherent and coherent processes is also reflected in the two types of linear and nonlinear processes. Linear systems are characterized by a proportionality between the input and output. Small disturbances cause small

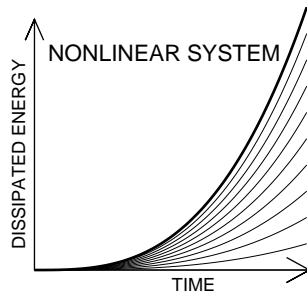
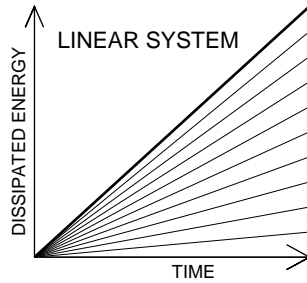


Figure 1: The output or dissipated energy in a linear system grows linearly with time, for a constant input rate (top left), while the output is highly unpredictable and not correlated with the input rate in a nonlinear dissipative system (bottom left). A practical example of a linear system is a hydroelectric plant, where the produced electric energy is proportional to the water input, as depicted with the water-storage dam at Yaotsu, Gifu, Japan (top right). A classical example of a dissipative nonlinear system is a snow avalanche, as shown in the large wet-snow avalanche at Deadman Canyon in the Sierra Nevada range (bottom right).

effects, and large disturbances are required to produce a large effect. A hydropower plant, for instance, produces electric energy that is proportional to the water inflow rate and gravitational or kinetic energy of the water that is feeding the turbine (Fig.1, top). Nonlinear processes, in contrast, are governed by a multiplicative or amplification factor, that leads to outputs of unpredictable magnitude, unlike linear systems. Small disturbances can cause both small or large avalanches. Classical examples are snow avalanches (Fig. 1, bottom), landslides, floodings, forest fires, or earthquakes.

A conceptual model to understand the basic nature of nonlinear processes was introduced by Bak, Tang, and Wiesenfeld (1987) in terms of sandpile avalanches. We can build a sandpile by dripping sand grains randomly with a more or less steady rate, until it forms a cone (Fig. 2, right). Once the sandpile reaches a critical slope (typically at an

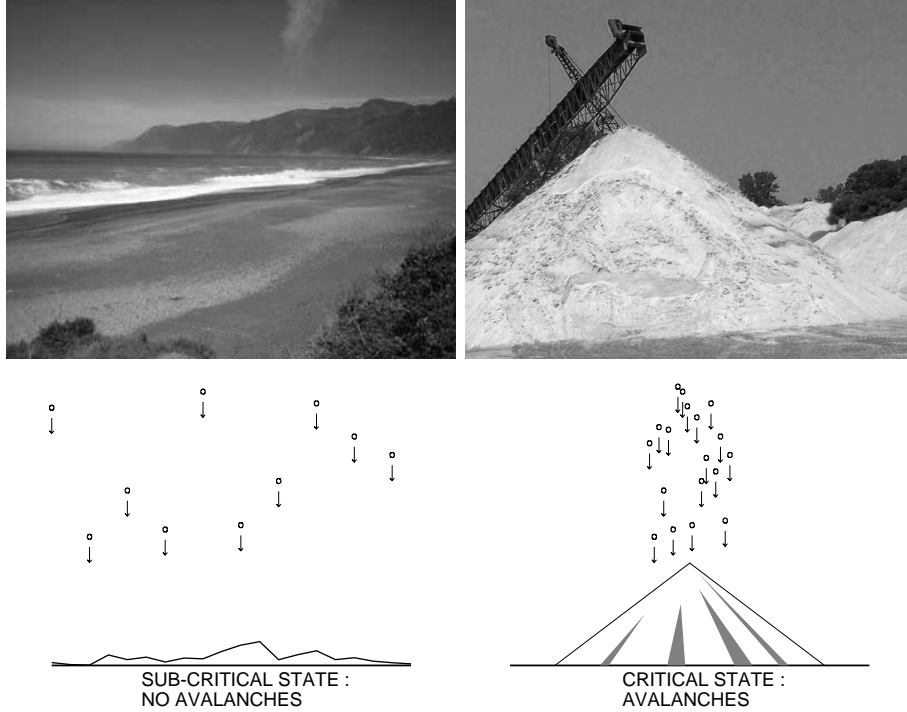


Figure 2: A static equilibrium produces no avalanche events (bottom left panel), such as the flat sand beach in northern California (top left panel), while randomly dripping sand onto a sandpile produces a state of self-organized criticality where avalanches occur (bottom right panel), such as with the conveyer belt of the Indian River Enterprises (top right panel).

angle of repose of  $\approx 34^\circ - 37^\circ$ ), avalanches occur in an unpredictable way, even when the input of dripped sand grains is steady. Bak called this driven state “*self-organized criticality*” (SOC), which has become a paramount characteristic of many nonlinear systems. A sand beach, in contrast, would be in a sub-critical state without avalanches (Fig. 2, left). The key features of nonlinear systems are powerlaw-like size distributions, which indicate scale-free parameter distributions, such as the size, time scale, or energy of an avalanche. The occurrence frequency distribution  $N(x)$  of a parameter  $x$  is defined as a powerlaw function when

$$N(x) \propto x^{-\alpha} . \quad (1)$$

The mathematical nature of such powerlaw distributions can easily be understood in terms of a coherent, exponential growth process as described in the following section.

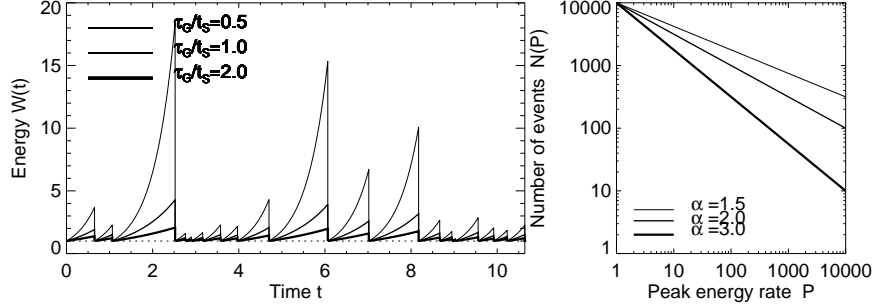


Figure 3: Time evolution of energy release rate  $W(t)$  for 3 different ratios of growth times to saturation times,  $\tau_G/t_S = (0.5, 1.0, 2.0)$  (left) and the corresponding powerlaw distributions of the peak energy release rate  $P$ . Note that the event set with the shortest growth time ( $\tau_G/t_S = 0.5$ ) reaches the highest energies and thus produces the flattest powerlaw slope ( $\alpha = 1 + \tau_G/t_S = 1.5$ ).

## 2 Analytical Model of SOC Avalanches

Avalanches occurring in the state of self-organized criticality represent local instabilities that grow explosively for some time interval. The released energy grows in a nonlinear way above some energy threshold, which can be parameterized by some nonlinear function, for instance by an exponential growth function. We define the time evolution of the energy release rate  $W(t)$  of a nonlinear process that starts at a threshold energy of  $W_0$  by

$$W(t) = W_0 \exp\left(\frac{t}{\tau_G}\right), \quad 0 \leq t \leq \tau, \quad (2)$$

where  $\tau_G$  represents the exponential growth time. The process grows exponentially until it saturates at time  $t = \tau$  with a saturation energy  $W_S$ ,

$$W_S = W(t = \tau) = W_0 \exp\left(\frac{\tau}{\tau_G}\right). \quad (3)$$

We define a peak energy release rate  $P$  that represents the maximum energy release rate  $W_S$ , after subtraction of the threshold energy  $W_0$ , that corresponds to the steady-state energy level before the nonlinear growth phase,

$$P = W_S - W_0 = W_0 \left[ \exp\left(\frac{\tau}{\tau_G}\right) - 1 \right]. \quad (4)$$

In the following, we will refer to the peak energy release rate  $P$  also briefly as “peak energy”. For the saturation times  $\tau$ , which we also call “rise times”, we assume a random probability distribution, approximated by an exponential function  $N(\tau)$  with e-folding time constant  $t_S$ ,

$$N(\tau)d\tau = \frac{N_0}{t_S} \exp\left(-\frac{\tau}{t_S}\right)d\tau. \quad (5)$$

This probability distribution is normalized to the total number of  $N_0$  events,

$$\int_0^\infty N(\tau)d\tau = N_0 . \quad (6)$$

In order to derive the probability distribution  $N(P)$  of peak energy release rates  $P$ , we have to substitute the variable of the peak energy,  $P$ , into the function of the rise time  $\tau(P)$ ,

$$N(P)dP = N(\tau)d\tau = N[\tau(P)] \left| \frac{d\tau}{dP} \right| dP . \quad (7)$$

This requires the inversion of the evolution function  $P(\tau)$  (Eq. 4),

$$\tau(P) = \tau_G \ln \left( \frac{P}{W_0} + 1 \right) , \quad (8)$$

and the calculation of its derivative  $d\tau/dP$ , which is

$$\frac{d\tau}{dP} = \frac{\tau_G}{W_0} \left( \frac{P}{W_0} + 1 \right)^{-1} . \quad (9)$$

Inserting the probability distribution of saturation times  $N(\tau)$  (Eq. 5), the inverted evolution function  $\tau(P)$  (Eq. 8) and its time derivative ( $d\tau/dP$ ) from Eq. (9) into the frequency distribution  $N(P)$  in Eq. (7) yields then,

$$N(P)dP = \frac{N_0(\alpha - 1)}{W_0} \left( \frac{P}{W_0} + 1 \right)^{-\alpha} dP , \quad (10)$$

which is an exact powerlaw distribution for large peak energies ( $P \gg W_0$ ) with a powerlaw slope  $\alpha$  of

$$\alpha = \left( 1 + \frac{\tau_G}{t_S} \right) . \quad (11)$$

The same mathematical result was derived in Rosner and Vaiana (1978), but the exponential growth was attributed to energy storage therein, rather than to the nonlinear growth phase of the instability here. The powerlaw slope thus depends on the ratio of the growth time to the e-folding saturation time, which is essentially the average number of growth times. Examples of time series with avalanches of different growth times ( $\tau_G/t_S = 0.5, 1.0, 2.0$ ) are shown in Fig. 3, along with the corresponding powerlaw distributions of peak energies  $P$ . Note that the fastest growing events produce the flattest powerlaw distribution of peak energies.

This simple model explains the powerlaw distribution of peak energies in nonlinear processes that have an exponential-like growth, which is the key characteristic of coherent processes. In incoherent processes, the growth time would be much larger than the average saturation time ( $\tau_G \gg t_S$ ), in which case the time evolution (Eq. 3) can be linearized, leading to  $P \propto \tau$  (Eq. 4), and the distribution of peak energies would be identical to that of the saturation times  $\tau$ , which is a Poissonian (exponential) distribution (Eq. 5) with a characteristic scale  $P \approx W_0$ . So, incoherent processes would have

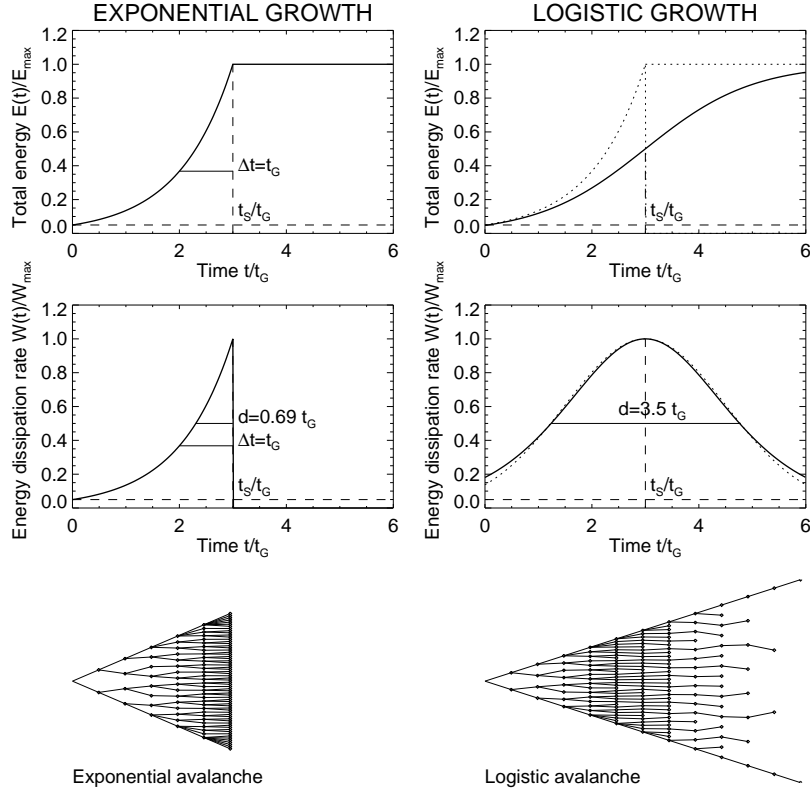


Figure 4: Time evolution of total released energy  $e(t)$  (top panels), the energy release rate  $W(t) = de(t)/dt$  (middle panels), and binary representation of avalanche growth rate (bottom panels), for both the exponential (left panels) and the logistic growth model (right panels). An exponential curve (right top) and a Gaussian curve (right middle) are drawn (with dotted lines) onto the logistic curves for comparison (Aschwanden et al. 1998).

the same exponential distribution of peak fluxes  $P$  as their random durations  $\tau$ ,

$$N^{inc}(P)dP = \frac{N_0}{W_0} \exp\left(-\frac{P}{W_0}\right)dP. \quad (12)$$

Therefore, we can use the functional shape of the occurrence frequency distribution of event sizes as a diagnostic of linear or nonlinear processes: exponential distribution functions indicate an incoherent random process, while powerlaw distribution functions indicate a coherent growth process.

The exponential-growth model represents just the mathematically simplest function to produce a powerlaw distribution of peak energies. It corresponds to a multiplicative process where the number of avalanche elements doubles every time step until it saturates (Fig. 4, left). The saturation phase, however, abruptly ends with a discontinuity. A more natural model is the logistic equation (discovered by Pierre Franois Verhulst

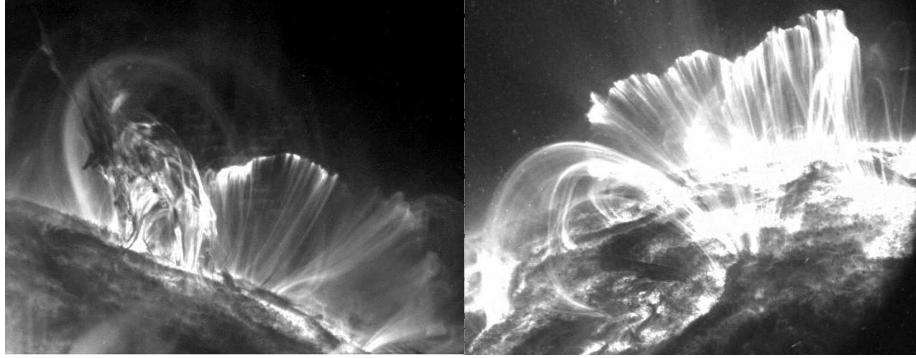


Figure 5: Solar flares observed in EUV with the TRACE spacecraft in 171 Å: The flare of 2001 Apr 15 exhibits an erupting filament in the foreground and a rising postflare arcade behind near the limb (left panel), while the 2000 Nov 9 flare displays the 3D geometry of the double-ribbon postflare arcade (right panel) [courtesy of NASA/TRACE].

in 1845), which is a first-order differential equation that approaches the saturation limit asymptotically,

$$\frac{dE(t)}{dt} = \frac{E(t)}{\tau_G} \cdot \left[ 1 - \frac{E(t)}{E_\infty} \right] \quad (13)$$

as shown in Fig. 4 (right). The time derivative, which mimics the energy release rate, has a maximum when the total energy has the steepest slope. The avalanche grows first exponentially and dies out gradually after the peak time of the fastest growth. It can be shown mathematically that the frequency distribution of the peak energies is also a powerlaw (Aschwanden et al. 1998), and thus this more physical description of a *logistic avalanche* with a continuous time evolution shares the same characteristic as an exponentially-growing avalanche, and thus both models can be used to describe SOC processes.

### 3 Solar Observations of SOC Phenomena

Solar flares are probably the best-studied datasets regarding SOC statistics in astrophysics. Solar flares are catastrophic events in the solar corona, most likely caused by a magnetic instability that triggers a magnetic reconnection process, producing emission in almost all wavelengths, such as in gamma-rays, hard X-rays, soft X-rays, extreme ultraviolet (EUV), H $\alpha$  emission, radio wavelengths, and sometimes even in white light. Two EUV images of solar flares are shown in Fig. 5, which display the intricate topology of the magnetic field produced at the beginning (Fig. 5, left) and end phase of the flare (Fig. 5, right). Since the emission mechanisms are all different in each wavelength, such as nonthermal bremsstrahlung (in hard X-rays), thermal bremsstrahlung (in soft X-rays and EUV), gyrosynchrotron emission (in microwaves), plasma emission (in metric and decimetric waves), etc., we expect that the calculation of energies

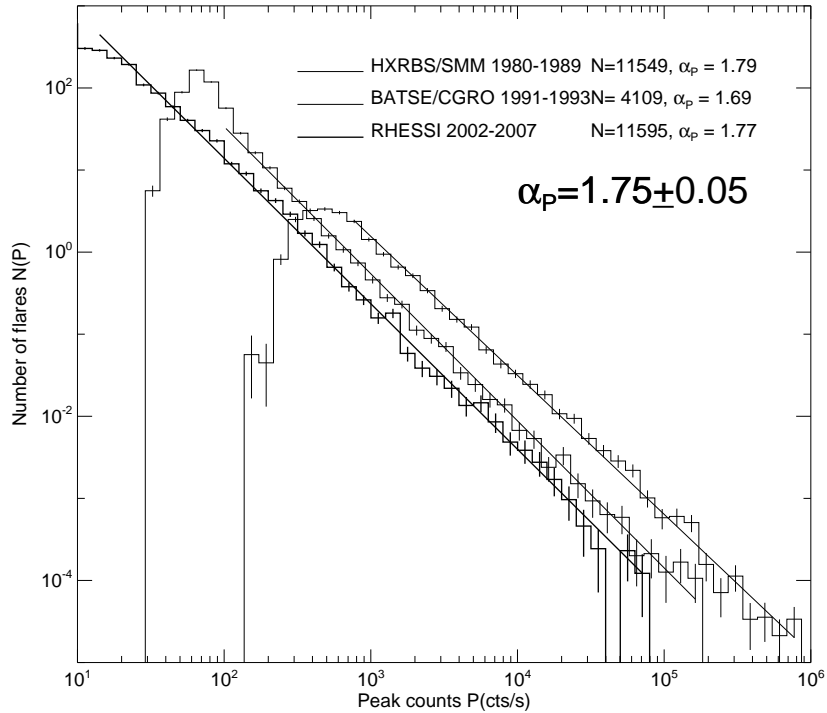


Figure 6: Occurrence frequency distributions of hard X-ray peak count rates  $P(cts/s)$  observed with HXRBS/SMM (1980-1989), BATSE (1991-1993), and RHESSI (2002-2007), with powerlaw fits. Note that BATSE/CGRO has larger detector areas, and thus records higher count rates.

contained in each event strongly depends on the emission mechanism, and thus on the wavelength. It is therefore advisable to investigate the statistics of SOC events in each wavelength domain separately. The most unambiguous SOC parameters to report are the peak flux  $P$ , the total flux or fluence  $E$ , defined as the time-integrated flux over the entire event, and the total time duration  $T$  of the event. Conversions of fluxes and fluences into energy release rates and total energies require physical models.

Statistics of the peak count rates  $P$  of over 20,000 solar flares observed in hard X-rays during three different space missions (SMM 1980-1989; CGRO 1991-1993; RHESSI 2002-2010) and during three different solar cycles have been gathered and their occurrence frequency distributions (or log N - log S distributions) are shown in Fig. 6. All three datasets show a near-perfect powerlaw distribution function with a mean slope of  $\alpha_P = 1.75 \pm 0.05$ . According to our model this value corresponds to a ratio of  $\tau_G/t_S = 0.75$  (Eq. 11) or a mean saturation time  $t_S/\tau_G = 1.33$  growth times. The distributions shown in Fig. 6 span together over 5 orders of magnitude, which means that the largest flare had a maximum saturation time of  $\ln(10^5) = 11.5$  growth times, which corresponds to an extremely coherent process that could never be



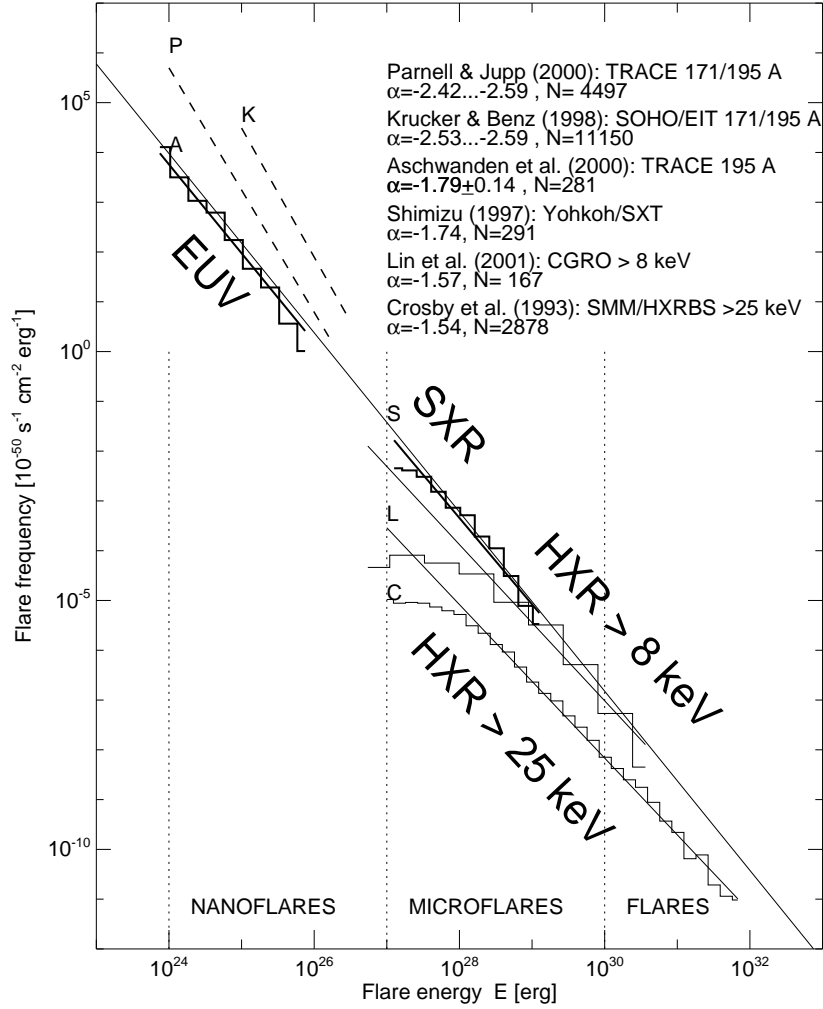


Figure 7: Composite flare frequency distribution in a normalized scale in units of  $10^{-50}$  flares per time unit ( $s^{-1}$ ), area unit ( $cm^{-2}$ ), and energy unit ( $erg^{-1}$ ). The energy is defined in terms of thermal energy  $E_{th} = 3n_e k_B T_e V$  for EUV and SXR, and in terms of non-thermal energy in  $> 25$  keV (Crosby et al. 1993) or  $> 8$  keV electrons (Lin et al. 2001). The slope of  $-1.8$  is extended over the entire energy domain of  $10^{24} - 10^{32}$  erg. The offset between the two HXR datasets is attributed to different lower energy cutoffs as well as different levels of flare activity during the observed time intervals [adapted from Aschwanden et al. 2000 and Lin et al. 2001].

explained by random probability.

Similar powerlaw-like occurrence frequency distributions have also been found for other flare parameters, such as the fluence, the flare duration, or flare energy (calculated from the thermal energy or energy in nonthermal hard X-ray producing electrons).

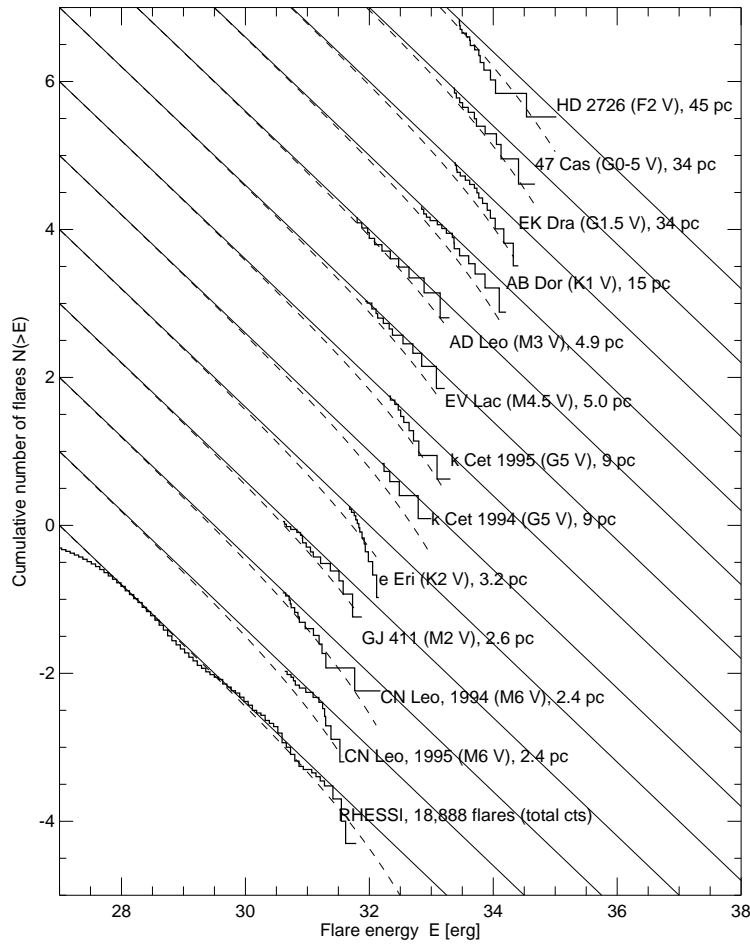


Figure 8: Cumulative occurrence frequency distributions  $N(> E)$  of stellar flares (vertically shifted for each star, in order of stellar distance) are shown as a function of the flare energy  $E$ , observed from 12 different stars by Audard et al. (2000). For comparison we show also the statistics of total hard X-ray emission of 18,888 solar flares observed with RHESSI, which covers an energy range of  $E \approx 10^{27.0} - 10^{31.7}$  ergs, while stellar flares have an energy range of  $E \approx 10^{30.7} - 10^{35.0}$  ergs. Note that most distributions show a (cumulative) powerlaw part with a slope of  $\alpha \approx 0.8$  (diagonal lines) at the low end and an exponential high-energy drop-off.

Based on this fact of scale-free powerlaw distributions, Lu and Hamilton (1991) were the first to apply the concept of self-organized criticality (SOC) to solar flares. With a cellular automaton model that mimics sandpile avalanches, they were able to simulate the size frequency distribution with a powerlaw slope of  $\alpha_P = 1.67 \pm 0.02$ , which is close to the observed value of  $\alpha_P = 1.75 \pm 0.05$  shown in Fig. 6.

The statistics of peak energies in solar flares has been extended to other wavelengths, from hard X-rays to soft X-rays and EUV and the powerlaw-like size distribu-

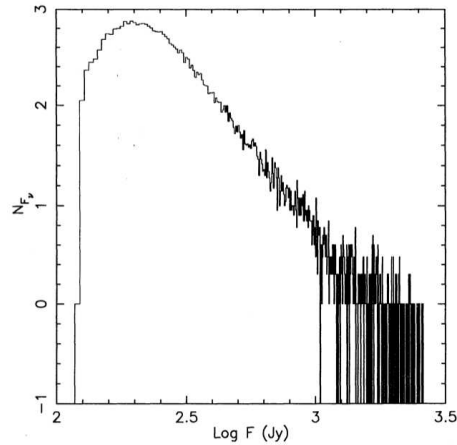


Figure 9: Frequency distribution of giant-pulse flux densities measured from the Crab pulsar, observed during 15-27 May 1991 with the Green Bank 43-m telescope at 1330, 800, and 812.5 MHz. The tail can be represented by a powerlaw distribution  $N_F \propto F^{-\alpha}$  with  $\alpha = 3.46 \pm 0.04$  for fluxes  $F > 200$  Jy (Lundgen et al. 1995).

tion has been found to extend over 8 orders of magnitude (Fig. 7). The events observed in soft X-rays have been called “*active region transients*”, having about 3-5 orders of magnitude less energy than the largest solar flare. The events observed in EUV have energies about 6-9 orders of magnitude less than the largest flare, and thus are called “*nanoflares*”. The self-similarity of flare parameters observed over this wide wavelength range, which implies also a large temperature range of  $T \approx (1 - 35) \times 10^6$  K, constitutes a powerful argument that the solar corona is in a state of self-organized criticality.

## 4 Astrophysical Observations of SOC Phenomena

Size distributions have also been sampled for stellar flares, although with much smaller statistics, typically  $\lesssim 15$  flare events per star. A comparison of size distributions from 12 flare stars (type F to M) observed by Audard et al. (2000) is shown in Fig. 8. Because of the smallness of the samples, the cumulative frequency distributions are shown, which have slope that is flatter by one compared with the differential frequency distribution ( $\alpha_P^{cum} = \alpha_P - 1$ ). The comparison in Fig. 8 demonstrates two important aspects: (1) stellar flares are up to two orders of magnitude more energetic ( $E \approx 10^{32} - 10^{34}$ ) than solar flares (see RHESSI comparison at bottom of Fig. 8), although the small sample implies common and relatively weak events, and (2) the drop-off at the upper bound of the cumulative frequency distribution yields a steeper slope than the powerlaw slope obtained from more complete frequency distributions. Correcting for the latter effect, stellar flares seem to have a similar powerlaw distribution as solar flares, and thus may be governed by the same SOC process.

Other size distributions with powerlaw shape have been observed in astrophysical data for pulsar glitches (e.g., Lundgren et al. 1995; shown in Fig. 9), for soft gamma-ray repeaters (e.g., Gogus et al. 1999), accretion disk objects around black hole candidates, such as Cygnus X-1 (e.g., Negoro et al. 1995), or for blazars (e.g., Ciprini et al. 2003). These astrophysical objects display size distributions with different powerlaw values, and thus can be explained by different physical processes, but the distribution type of a powerlaw function constitutes a powerful argument that the underlying system is driven into the critical state of self-organized criticality, which is common to earthquakes, sunquakes (occurring during large flares), and neutron star quakes (pulsar glitches).

*Acknowledgements: This work is partially supported by NASA contract NAS5-98033 of the RHESSI mission through University of California, Berkeley (subcontract SA2241-26308PG) and NASA grant NNX08AJ18G. We acknowledge access to solar mission data and flare catalogs from the Solar Data Analysis Center(SDAC) at the NASA Goddard Space Flight Center (GSFC).*

## References

- Aschwanden, M.J., Dennis, B.R., and Benz, A.O. 1998, *Logistic avalanche processes, elementary time structures, and frequency distributions of flares*, *Astrophys. J.* **497**, 972-993.
- Aschwanden, M.J., Tarbell, T., Nightingale, R., Schrijver, C.J., Title, A., Kankelborg, C.C., Martens, P.C.H., and Warren, H.P. 2000, *Time variability of the quiet Sun observed with TRACE: II. Physical parameters, temperature evolution, and energetics of EUV nanoflares*, *Astrophys. J.* **535**, 1047-1065.
- Audard, M., Guedel, M., Drake, J.J., and Kashyap, V.L. 2000, *Extreme-ultraviolet flare activity in late-type stars* *Astrophys. J.* **541**, 396-409.
- Bak, P., Tang, C., & Wiesenfeld, K. 1987, *Self-organized criticality - An explanation of 1/f noise*, *Physical Review Lett.* **59/27**, 381-384.
- Ciprini, S., Fiorucci, M., Tosti, G., and Marchili, N. 2003, *The optical variability of the blazar GV 0109+224. Hints of self-organized criticality*, in *High energy blazar astronomy*, ASP Conf. Proc. **229**, (eds. L.O. Takalo and E. Valtaoja), ASP: San Francisco, p.265.
- Crosby, N.B., Aschwanden, M.J., and Dennis, B.R. 1993, *Frequency distributions and correlations of solar hard X-ray flare parameters*, *Solar Phys.* **143**, 275-299.
- Gogus, E., Woods, P.M., Kouveliotou, C., van Paradijs, J., Briggs, M.S., Duncan, R.C., and Thompson, C. 1999, *Statistical properties of SGR 1900+14 bursts*, *Astrophys. J.* **526**, L93-L96.
- Krucker, S. and Benz, A.O. 1998, *Energy distribution of heating processes in the quiet solar corona*, *Astrophys. J.* **501**, L213-L216.
- Lin, R.P., Feffer, P.T., and Schwartz, R.A. 2001, *Solar Hard X-Ray Bursts and Electron Acceleration Down to 8 keV*, *Astrophys. J.* **557**, L125-L128.
- Lu, E.T. and Hamilton, R.J. 1991, *Avalanches and the distribution of solar flares*, *Astrophys. J.* **380**, L89-L92.
- Lundgren, S.C., Cordes, J.M., Ulmer, M., Matz, S.M., Lomatch, S., Foster, R.S., and Hankins, T. 1995, *Giant pulses from the Crab pulsar: A joint radio and gamma-ray study*, *Astrophys. J.* **453**, 433-445.
- Negoro, H., Kitamoto, S., Takeuchi, M., and Mineshige, S. 1995, *Statistics of X-ray fluctuations from Cygnus X-1: Reservoirs in the disk ?*, *Astrophys. J.* **452**, L49-L52.
- Parnell, C.E. and Jupp, P.E. 2000, *Statistical analysis of the energy distribution of nanoflares in the quiet Sun*, *Astrophys. J.* **529**, 554-569.
- Rosner, R., and Vaiana, G.S. 1978, *Cosmic flare transients: constraints upon models for energy storage and release derived from the event frequency distribution*, *Astrophys. J.* **222**, 1104-1108.
- Shimizu, T. and Tsuneta, S. 1997, *Deep survey of solar nano-flares with Yohkoh*, *Astrophys. J.* **486**, 1045-1057.